

Novel OFDM Based on C-Transform for Improving Multipath Transmission

Hussein A. Leftah and Said Boussakta, *Senior Member, IEEE*

Abstract—In this paper, a new orthogonal-frequency-division multiplexing using the C-transform (C-OFDM) is introduced. An exact closed-form bit-error rate (BER) is derived for the proposed C-OFDM system over multipath channels and different kinds of modulation formats. The BER performance of the proposed C-OFDM is evaluated by mathematics and simulation for different channel models, modulation formats, under zero-padding (ZP) and minimum mean-square-error (MMSE) detection. The results are then compared with those of the discrete cosine transform (DCT) and discrete Fourier transform (DFT)-based OFDM, showing that over multipath channel, the new C-OFDM has better BER performance than both the DCT-OFDM and the DFT-OFDM. The proposed scheme is also found to achieve some reduction in the peak-to-average power ratio (PAPR) in comparison with the aforementioned OFDM schemes as the block-diagonal-structure (BDS) property of the C-transform minimizes the input signal superposition. The proposed system has the merits of being resilience to multipath channel dispersion and relatively has lower PAPR.

Index Terms—C-transform, discrete cosine transform (DCT), discrete Fourier transform (DFT), orthogonal frequency division multiplexing (OFDM), bit-error rate (BER), peak-to-average power ratio (PAPR).

I. INTRODUCTION

HERE, has been growing interest in multicarrier modulation based on orthogonal frequency division multiplexing (OFDM) that adopts discrete Fourier transform (DFT) or its fast algorithm (FFT) counterpart as a modulation scheme [1]–[7]. With the ability to mitigate the effects of multipath fading and delay spread of radio channels, OFDM has been adopted in many applications and standards, for instance, (IEEE 802.11a/g/n), metropolitan area networks (IEEE 802.16a) and (HIPERLAN/2) as well as wire-line digital communications

Manuscript received December 03, 2013; revised June 17, 2014; accepted September 15, 2014. Date of publication October 08, 2014; date of current version November 05, 2014. The associate editor coordinating the review of this manuscript and approving it for publication was Prof. Joseph Cavallaro. This work was supported in part by EPSRC under grant EP/11004637/1 and Leverhulme Trust under grant number VP1-2012-008.

H. A. Leftah is with the Electrical Department, Technical Engineering School, Southern Technical University, Basrah, 61004, Iraq (e-mail: h.a.leftah@gmail.com).

S. Boussakta is with the School of Electrical and Electronic Engineering, Newcastle University, Newcastle upon Tyne, NE1 7RU, U.K. (e-mail: said.boussakta@ncl.ac.uk).

Color versions of one or more of the figures in this paper are available online at <http://ieeexplore.ieee.org>.

Digital Object Identifier 10.1109/TSP.2014.2362097

systems, such as asymmetric digital subcarrier loop (ADSL) [8], [9] and power line communications (PLC) [10], [11].

Multipath frequency-selective fading channels have a deleterious effects on the bit-error-rate (BER) performance of the OFDM. Therefore, a large number of techniques have been developed to mitigate the detrimental effect of the frequency-selective multipath fading channels in wireless communications including power allocation [12]. Though the power allocation technique seems theoretically effective, it suffers from two practical drawbacks. The first problem is that the high dynamic power range at the transmitter to attain the instantaneous channel requirements demands a costly power amplifier. The second is the high complexity as channel state information (CSI) must be available at the transmitter. Ideally, the BER performance improvement should not be achieved by increasing the transmit power or adding costly equipments as it hinders the high speed wireless communications which are crucially demanded for future multimedia communications.

Another method using the discrete cosine transform (DCT) as an alternative to the DFT for multicarrier communication schemes has been investigated [13]–[19] which has been found to offer certain advantages [20]–[24]. The DCT-OFDM is less sensitive to the carrier frequency offset (CFO) than the DFT-OFDM. Moreover, as DCT is a real transform, the DCT-OFDM can avoid the in-phase/quadrature phase (IQ) imbalance when the data mapping is real [20] and [24].

In this paper, the C-transform proposed in [25] is utilized to implement a new OFDM modulation scheme called the C-OFDM. The new system retain the advantages of the DCT-OFDM, over DFT-OFDM described in [20] and reduces the BER and peak-to-average power ratio (PAPR) substantially. A mathematical expression for the BER performance of the proposed C-OFDM scheme, which tightly matches the simulation results, is derived in this work. In comparison to the DCT-OFDM and the DFT-OFDM, the proposed C-OFDM achieves significant transmission improvement. Over multipath channels, the proposed C-OFDM system achieves about 10 dB SNR gain at 10^{-4} BER performance over both the DCT-OFDM and DFT-OFDM. This is attributed to the fact that the information symbol is spread out over other subcarriers by the C-transform where it can be recovered at the receiver from the unaffected subcarriers even when it is carried on greatly attenuated subcarrier, mitigating the deleterious effect of deep notches in the channel spectral. However, this phenomenon does not exhibit in the DFT-OFDM and the DCT-OFDM counterparts as the information on subcarrier that corresponding to

deep narrowband notch will be completely wiped out. Furthermore, the proposed system is found to preserve the average power and reduces the peak value, hence reduces the PAPR of the transmitted signal by more than 3 dB in comparison with the DCT-OFDM and DFT-OFDM systems. This is due to the block-diagonal-structure (BDS) property of the C-transform reducing the signal superposition, which is the main cause for the high peaks in multicarrier systems. The new C-OFDM is based on real C-transform, so it inherits the same characteristics of the DCT-OFDM system with more added advantages such as the enhanced signal diversity and some reduction in the PAPR. Moreover, it can also be used with complex valued constellation as it is shown in this paper for the M-phase-shift keying (PSK) and the M-quadrature amplitude modulation (QAM) mapping.

Using the proposed C-OFDM for baseband transmission systems such as the DSL, a certain spectral efficiency can be achieved with real PAM unconstrained. In contrast, to achieve the same spectral efficiency by using the DFT-OFDM, the complex QAM information block is forced to be conjugate symmetric to ensure a real valued inverse DFT output at the transmitter which requires more receiver complexity. When a real-valued modulation formats, for instance, BPSK or pulse-amplitude-modulation (PAM) are used, the C-OFDM system can avoid IQ imbalance problems discussed in [26], which are considered as weaknesses in the DFT-OFDM. Moreover, if the modulation format is real, single-sideband (SSB) transmission technology would be applicable in the case of our proposed OFDM system. However, this would not be possible in the case of the DFT-OFDM system as the IFFT of real data is complex [20].

The rest of this paper is organized as follows. Mathematical analysis is first given for the proposed scheme in Section II. Section III elaborates the transmission analysis and the BER calculations of the proposed C-OFDM over multipath fading channels with zero-padding (ZP) and MMSE detection. The zero padding (ZP) C-OFDM (ZP-C-OFDM) is more robust to frequency-selective multipath fading channels than both the ZP-DCT-OFDM and ZP-DFT-OFDM systems due to the C-transform, hence, increases the transmitted signal diversity. Section IV presents The mathematical analysis for the PAPR of the proposed C-OFDM and the solid-state power amplifier (SSPA) model, showing that the proposed scheme has the lowest PAPR compared to the aforementioned schemes as the inherent block diagonal structure (BDS) of the C-transform reduces the number of data symbols that perform each OFDM sample. Section V presents the computational complexity. Section VI presents the simulation results in the standards context of the ITU pedestrian and vehicular channel models. Finally, our conclusions are drawn in Section VI.

II. PROPOSED SYSTEM ANALYSIS

Henceforth, the following notations will be used in this paper: The term C-OFDM refers to our proposed C-transform based OFDM system, DCT-OFDM refers to the DCT based OFDM

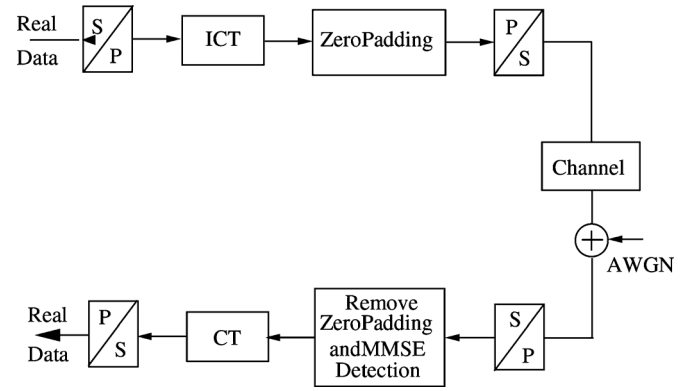


Fig. 1. C-OFDM system block diagram when real signalling is used.

and DFT-OFDM refers to DFT based OFDM. The notation \mathbf{Q} is used to represent the $N \times N$ Walsh Hadamard matrix while the notation \mathbf{D} represents the $N \times N$ type II discrete cosine matrix which is given as $\mathbf{D}_{kn} = \sqrt{\frac{2}{N}} \kappa_n \cos(\frac{\pi(2k+1)n}{2N})$ where κ_n is equal to 1 only when $n = 0$ and equal to $\frac{1}{\sqrt{2}}$ otherwise. x^I and x^Q denote the in-phase and quadrature-phase components of x respectively. The notation \mathbf{I}_N represents the identity matrix of dimension N and $\mathbf{L}_{zp} = [\mathbf{I}_N \mathbf{0}_{N \times L_G}]^T$ is an $M \times N$ zero-padding matrix. The function $E[x]$ denotes the expected value of a random variable x . The symbol $(\cdot)^T$ denotes the transpose operation whilst $(\cdot)^H$ denotes the Hermitian operator. Ultimately, $\text{tr}(\cdot)$ represents the trace operation.

The proposed C-OFDM system block diagram for real and complex data format is shown in Figs. 1 and 2 respectively. It shows that the ZP guard interval scheme is used instead of the conventional cyclic prefix (CP). Unlike the scheme in [15], the zero-padding scheme can compensate for the channel effects without doubling the transmitted symbol. The transmitted sequence is zero padded with a sequence that is no less than the length of the channel impulse response. The use of zero-padding scheme in the case of the DFT-OFDM has been addressed in [27]; which showed that it can achieve better BER performance than the cyclic prefix DFT-OFDM scheme because the data symbols can be recovered regardless of the channel zero locations. Consequently, in this paper we use the zero padding scheme. The C-OFDM system block diagram for real data is shown in Fig. 1 and for complex data is shown in Fig. 2. A minimum mean square-error (MMSE) equalizer [20] is used in the receiver to compensate for the channel effect. The MMSE receiver of the C-OFDM, DCT-OFDM and DFT-OFDM with ZP guard interval have the same degree of complexity.

Based on a specific constellation format in the data encoder, the input data is first mapped into real or complex modulated symbols X_m , ($m = 0, 1, 2, \dots, N-1$). In vector form, each block of data symbols is represented as

$$\mathbf{X}^T = [X_0, X_1, \dots, X_{N-1}], \quad (1)$$

where $(\cdot)^T$ denotes the transpose operation, which is the same for real and imaginary parts of the complex symbol and \mathbf{X} is an

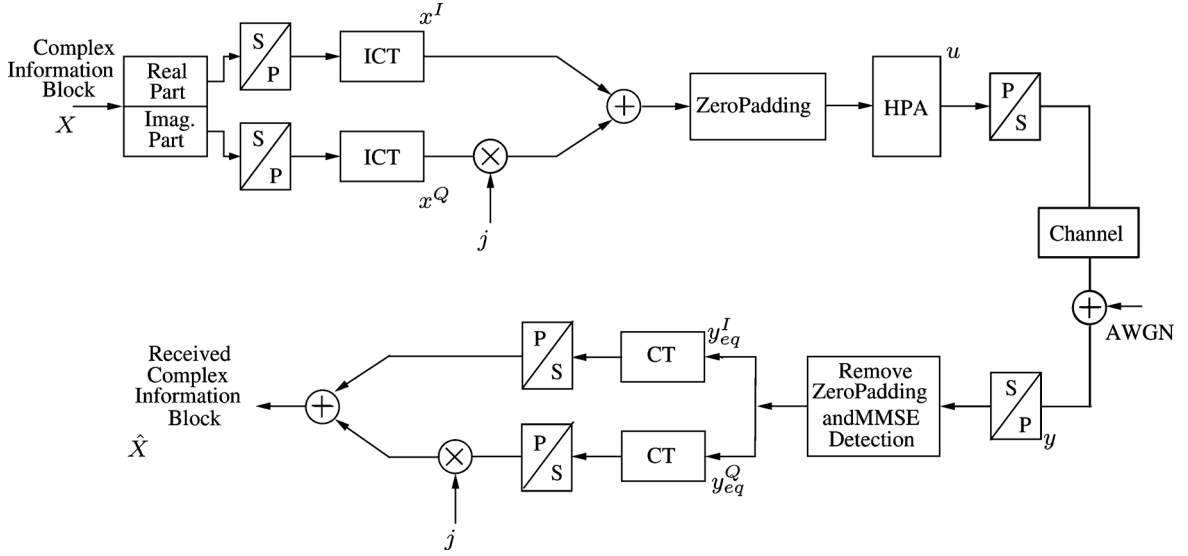


Fig. 2. C-OFDM system block diagram when complex signalling is used.

$N \times 1$ vector. Then these N information symbols modulate N different subcarriers by using inverse \mathbf{C} transform (ICT). The resulting samples would be expressed as follows: At first, the information symbols are processed as

$$s_n = \frac{1}{\sqrt{N}} \sum_{m=0}^{N-1} X_m (-1)^{\mu_{m,n}}, \quad (2)$$

where

$$\mu_{m,n} = \sum_{j=1}^{N_1} m_j \odot n_j. \quad (3)$$

In (3), $m_j \odot n_j$ denotes the j th bit-by-bit product of binary representation of the integers m_j and n_j (AND operation between the bits of the binary representation of m and n) while $N_1 = \log_2 N$, is the number of binary digits in each index. The output samples then modulate N different subcarriers as

$$\begin{aligned} x_k &= \frac{1}{\sqrt{N}} \sum_{n=0}^{N-1} s_n \hat{D}_{kn}, \\ &= \frac{1}{N} \sum_{n=0}^{N-1} \sum_{m=0}^{N-1} X_m (-1)^{\mu_{m,n}} \hat{D}_{kn}. \end{aligned} \quad (4)$$

In (4), \hat{D}_{kn} is the k th row and n th column element of the $\hat{\mathbf{D}}^T$ matrix and it is given as

$$\hat{\mathbf{D}} = \mathbf{\Gamma} \mathbf{D}^T \mathbf{\Phi}, \quad (5)$$

where $\mathbf{\Gamma}$ is the Gray-reverse-order (GRO) matrix where each two successive values differ in only one bit, and $\mathbf{\Phi}$ represents the

bit-reverse-order (BRO) matrix respectively. In what follows, (4) can be written as

$$\begin{aligned} x_k &= \frac{1}{N} \sum_{m=0}^{N-1} X_m \sum_{n=0}^{N-1} (-1)^{\mu_{m,n}} \hat{D}_{kn}, \\ &= \frac{1}{N} \sum_{m=0}^{N-1} X_m C_{km}, \end{aligned} \quad (6)$$

where $C_{km} = \sum_{n=0}^{N-1} (-1)^{\mu_{m,n}} \hat{D}_{kn}$ is the k th row and m th column element of the inverse \mathbf{C} transform. Thus (4) can be written in matrix form as

$$\begin{aligned} \mathbf{x} &= \hat{\mathbf{D}}^T \mathbf{Q} \mathbf{X}, \\ &= \mathbf{C}^T \mathbf{X}. \end{aligned} \quad (7)$$

In (7), \mathbf{x} is an $N \times 1$ vector represents the OFDM symbol and \mathbf{Q}_N denotes the Walsh-Hadamard matrix of order N . It is worth mentioning here that the GRO of the rows and BRO of the columns are applied to the \mathbf{D}^T to derive the fast algorithm for the ICT. Consequently, the \mathbf{D}^T can be written as a function of its lower order matrices as

$$\hat{\mathbf{D}}_N^T = \begin{bmatrix} \mathbf{J}_{\frac{N}{2}} & \mathbf{J}_{\frac{N}{2}} \\ \mathbf{K}_{\frac{N}{2}} & -\mathbf{K}_{\frac{N}{2}} \end{bmatrix}. \quad (8)$$

On the other hand, \mathbf{Q} of size $N = 2^P$, where P is an integer, can be expressed as

$$\begin{aligned} \mathbf{Q}_N &= \otimes_{i=1}^P \mathbf{Q}_2, \\ &= \overbrace{\mathbf{Q}_2 \otimes \mathbf{Q}_2 \otimes \cdots \otimes \mathbf{Q}_2}^P, \end{aligned} \quad (9)$$

where $\mathbf{Q}_2 = \begin{bmatrix} 1 & 1 \\ 1 & -1 \end{bmatrix}$ while \otimes is a Kronecker product. Accordingly, the WHT can be written in lower order as

$$\mathbf{Q}_N = \begin{bmatrix} \mathbf{Q}_{\frac{N}{2}} & \mathbf{Q}_{\frac{N}{2}} \\ \mathbf{Q}_{\frac{N}{2}} & -\mathbf{Q}_{\frac{N}{2}} \end{bmatrix}. \quad (10)$$

Therefore the ICT can be written as

$$\mathbf{C}_N = \begin{bmatrix} 2\mathbf{J}_{\frac{N}{2}} \mathbf{Q}_{\frac{N}{2}} & 0 \\ 0 & 2\mathbf{K}_{\frac{N}{2}} \mathbf{Q}_{\frac{N}{2}} \end{bmatrix}. \quad (11)$$

For clarity and without loss of generality, the ICT IDCT and IDFT matrices for $N = 8$ and $N = 16$ are shown in (12)–(16), shown at the bottom of this page and the next page.

From (12) and (15), it is clear that the ICT matrix has a block-diagonal structure (BDS) with two-third of its elements being zero. Also the C matrix of order N differs from the C matrix of order N/2 only by the lower part of the block diagonal structure. These characteristics of the C-transform make it advantageous in term of PAPR, BER and scalability as will be shown analytically in Sections III and IV and by simulation in Section V.

For the case of the DCT matrices of size 8 and 16 shown in (13) and (16) and DFT of size 8 shown in (14), these matrices are full with non zero elements. The DCT or DFT matrices of order N/2 are completely different for their matrices of order N. Also, all the elements of the first row of the DCT or DFT has the same amplitude and phase. This could lead to high PAPR when all the data symbols are aligned in phase.

III. TRANSMISSION ANALYSIS

The C-OFDM system block diagram for complex data format is shown in Fig. 2. It can be observed that for a complex constellation, ICT must be used twice in both transmitter and receiver:

one for the real part and the other for the imaginary part of the information symbols. However, it is used only once when the data are drawn from real modulation format such as BPSK or PAM as shown in Fig. 1. For fair comparison with DFT-OFDM, during this work, we will focus on complex constellation such as QPSK and 16-QAM modulation formats. However, it should be noted that the C-OFDM and DCT-OFDM are better suited for real data than the DFT-OFDM.

Therefore, we consider block-by-block transmission where the information symbols are divided into blocks, each of length N . Temporarily, we will talk about the real part only (in-phase component \mathbf{x}^I), as the same procedures are applied to the imaginary part (quadrature-phase component \mathbf{x}^Q). The C-OFDM symbol after ICT can be expressed as

$$\mathbf{x}^I = \mathbf{C}^T \mathbf{X}^I. \quad (17)$$

The power spectral density (PSD) of the proposed C-OFDM has the same shape and bandwidth as that of the DCT-OFDM as shown in Fig. 3. A zero padding sequence of length L_G samples, greater than or equal to maximum access delay of the multipath channel, is then appended to the end of the transmitted signal to prevent the inter-symbol interference (ISI). The resulting $M \times 1$ vector, $M = N + L_G$, is then given as

$$\begin{aligned} \mathbf{u}^I &= \mathbf{L}_{zp} \mathbf{x}^I, \\ \mathbf{u}^Q &= \mathbf{L}_{zp} \mathbf{x}^Q, \end{aligned} \quad (18)$$

$$\mathbf{C}_8 = \begin{bmatrix} 1 & 0 & 0 & 0 & 0 & 0 & 0 & 0 \\ 0 & 1 & 0 & 0 & 0 & 0 & 0 & 0 \\ 0 & 0 & 0.9239 & 0.3827 & 0 & 0 & 0 & 0 \\ 0 & 0 & -0.3827 & 0.9239 & 0 & 0 & 0 & 0 \\ 0 & 0 & 0 & 0 & 0.9061 & -0.0747 & 0.3753 & 0.1802 \\ 0 & 0 & 0 & 0 & 0.2126 & 0.7682 & -0.5133 & 0.3182 \\ 0 & 0 & 0 & 0 & -0.3182 & 0.5133 & 0.7682 & 0.2126 \\ 0 & 0 & 0 & 0 & -0.1802 & -0.3753 & -0.0747 & 0.9061 \end{bmatrix}, \quad (12)$$

$$\mathbf{DCT}_8 = \begin{bmatrix} 0.3536 & 0.3536 & 0.3536 & 0.3536 & 0.3536 & 0.3536 & 0.3536 & 0.3536 \\ 0.4904 & 0.4157 & 0.2778 & 0.0975 & -0.0975 & -0.2778 & -0.4175 & -0.4904 \\ 0.4619 & 0.1913 & -0.1913 & -0.4619 & -0.4619 & -0.1913 & 0.1913 & 0.4619 \\ 0.4157 & -0.0975 & -0.4904 & -0.2778 & 0.2778 & 0.4904 & 0.0975 & -0.4157 \\ 0.3536 & -0.3536 & -0.3536 & 0.3536 & 0.3536 & -0.3536 & -0.3536 & 0.3536 \\ 0.2778 & -0.4904 & 0.0975 & 0.4157 & -0.4157 & -0.0975 & 0.4904 & -0.2778 \\ 0.1913 & -0.4619 & 0.4619 & -0.1913 & -0.1913 & 0.4619 & -0.4619 & 0.1913 \\ 0.0975 & -0.2778 & 0.4157 & -0.4904 & 0.4904 & -0.4157 & 0.2778 & -0.0975 \end{bmatrix}, \quad (13)$$

$$\mathbf{DFT}_8 = \frac{1}{\sqrt{8}} \begin{bmatrix} 1 & 1 & 1 & 1 & 1 & 1 & 1 & 1 \\ 1 & 0.7 + j0.7 & -j & -0.7 - j0.7 & -1 & -0.7 + j0.7 & j & 0.7 + j0.7 \\ 1 & -j & -1 & j & 1 & -j & -1 & j \\ 1 & -0.7 - j0.7 & j & 0.7 - j0.7 & -1 & 0.7 + j0.7 & -j & -0.7 + j0.7 \\ 1 & -1 & 1 & -1 & 1 & -1 & 1 & -1 \\ 1 & -0.7 + j0.7 & -j & 0.7 + j0.7 & -1 & 0.7 - j0.7 & j & -0.7 - j0.7 \\ 1 & j & -1 & -j & 1 & j & -1 & -j \\ 1 & 0.7 + j0.7 & j & -0.7 + j0.7 & -1 & -0.7 - j0.7 & -j & 0.7 - j0.7 \end{bmatrix}, \quad (14)$$

where, \mathbf{I}_N is an $N \times N$ identity matrix, $\mathbf{0}_{N \times L_G}$ is an $N \times L_G$ matrix with zero elements and $\mathbf{L}_{zp} = (\mathbf{I}_N \mathbf{0}_{N \times L_G})^T$ is an $M \times N$ zero-padding matrix. The transmitted signal then passes through a channel. Assume that the channel is $L+1$ taps channel, $h_k = 0$ for all indexes out of the interval ($0 \leq k \leq L$). The received signal is the convolution of the transmitted signal, $\mathbf{u} = \mathbf{u}^I + j\mathbf{u}^Q$, with the channel impulse response h corrupted by additive white Gaussian noise (AWGN) and can be written as

$$y_k = u_k \otimes h_k + v_k, \\ = \sum_{d=0}^L u_{k-d} h_d + v_k, \quad (19)$$

where \otimes denotes the convolution operation and v is the AWGN noise with zero-mean and variance $\sigma_v^2 = E[v_k^2]$. Equation (19) can be rewritten in more expressive way in matrix form as

$$\mathbf{y} = \mathbf{H}_0 \mathbf{u} + \mathbf{v}, \quad (20)$$

where $\mathbf{u} = \mathbf{u}^I + j\mathbf{u}^Q$, $\mathbf{y} = \mathbf{y}^I + j\mathbf{y}^Q$ and $\mathbf{v} = \mathbf{v}^I + j\mathbf{v}^Q$ are $M \times 1$ vectors; \mathbf{H}_0 is an $M \times M$ channel convolutional matrix which is Toeplitz and defined in [28]; its elements i_{th} , $0 \leq i \leq M-1$, row and k_{th} , $0 \leq k \leq M-1$, column are given as $H_0(i, k) = h(i-k)$ for $0 \leq (i-k) \leq L$ and $H_0(i, k) = 0$ otherwise. Thus, \mathbf{H}_0 matrix can be written as

$$\mathbf{H}_0 = \begin{bmatrix} h_0 & 0 & 0 & 0 & \dots & \dots & 0 & 0 \\ h_1 & h_0 & 0 & 0 & \dots & \dots & 0 & 0 \\ 0 & h_1 & h_0 & 0 & \dots & \dots & 0 & 0 \\ \dots & \dots & h_1 & \dots & \dots & \dots & 0 & 0 \\ h_L & \dots & \dots & \dots & \dots & \dots & \vdots & \dots \\ 0 & h_L & \dots & \dots & \dots & \dots & \dots & \dots \\ 0 & 0 & \dots & \dots & \dots & \dots & \dots & \dots \\ \vdots & \vdots & \dots & \dots & \dots & \dots & h_1 & h_0 & 0 \\ 0 & 0 & \dots & 0 & h_L & \dots & \dots & h_1 & h_0 \end{bmatrix}. \quad (21)$$

$$\mathbf{C}_{16} = \begin{bmatrix} 1 & 0 & 0 & 0 & 0 & 0 & 0 & 0 & 0 & 0 & 0 & 0 & 0 & 0 & 0 & 0 \\ 0 & 1 & 0 & 0 & 0 & 0 & 0 & 0 & 0 & 0 & 0 & 0 & 0 & 0 & 0 & 0 \\ 0 & 0 & 0.9239 & 0.3827 & 0 & 0 & 0 & 0 & 0 & 0 & 0 & 0 & 0 & 0 & 0 & 0 \\ 0 & 0 & -0.3827 & 0.9239 & 0 & 0 & 0 & 0 & 0 & 0 & 0 & 0 & 0 & 0 & 0 & 0 \\ 0 & 0 & 0 & 0 & 0.9061 & -0.0747 & 0.3753 & 0.1802 & 0 & 0 & 0 & 0 & 0 & 0 & 0 & 0 \\ 0 & 0 & 0 & 0 & 0.2126 & 0.7682 & -0.5133 & 0.3182 & 0 & 0 & 0 & 0 & 0 & 0 & 0 & 0 \\ 0 & 0 & 0 & 0 & -0.3182 & 0.5133 & 0.7682 & 0.2126 & 0 & 0 & 0 & 0 & 0 & 0 & 0 & 0 \\ 0 & 0 & 0 & 0 & -0.1802 & -0.3753 & -0.0747 & 0.9061 & 0 & 0 & 0 & 0 & 0 & 0 & 0 & 0 \\ 0 & 0 & 0 & 0 & 0 & 0 & 0 & 0 & 0.9081 & -0.0177 & -0.0743 & -0.0368 & 0.3735 & -0.0073 & -0.1794 & 0.0888 \\ 0 & 0 & 0 & 0 & 0 & 0 & 0 & 0 & 0.1143 & 0.7004 & 0.2381 & -0.0577 & 0.0474 & 0.2901 & -0.5748 & 0.1393 \\ 0 & 0 & 0 & 0 & 0 & 0 & 0 & 0 & 0.1875 & -0.1500 & 0.6775 & 0.2420 & -0.4527 & 0.3621 & 0.2806 & 0.1002 \\ 0 & 0 & 0 & 0 & 0 & 0 & 0 & 0 & 0.0924 & 0.2035 & -0.1490 & 0.7351 & -0.2230 & -0.4912 & -0.0617 & 0.3045 \\ 0 & 0 & 0 & 0 & 0 & 0 & 0 & 0 & -0.3045 & 0.0617 & 0.4912 & 0.2230 & 0.7531 & -0.1490 & 0.2035 & 0.0924 \\ 0 & 0 & 0 & 0 & 0 & 0 & 0 & 0 & -0.1002 & -0.2806 & -0.3621 & 0.4527 & 0.2420 & 0.6775 & -0.1500 & 0.1875 \\ 0 & 0 & 0 & 0 & 0 & 0 & 0 & 0 & -0.1393 & 0.5748 & -0.2901 & -0.0474 & -0.0577 & 0.2381 & 0.7004 & 0.1143 \\ 0 & 0 & 0 & 0 & 0 & 0 & 0 & 0 & -0.0888 & -0.1794 & 0.0073 & -0.3735 & -0.0368 & -0.0743 & -0.0177 & 0.9018 \end{bmatrix}. \quad (15)$$

$$\mathbf{DCT}_{16} = \begin{bmatrix} 0.25 & 0.25 & 0.25 & 0.25 & 0.25 & 0.25 & 0.25 & 0.25 & 0.25 & 0.25 & 0.25 & 0.25 & 0.25 & 0.25 & 0.25 & 0.25 \\ 0.319 & 0.3383 & 0.3118 & 0.2733 & 0.2243 & 0.1667 & 0.1026 & 0.0347 & -0.0347 & -0.1026 & -0.1667 & -0.2243 & -0.2733 & -0.3118 & -0.3383 & -0.3519 \\ 0.3468 & 0.2940 & 0.1964 & 0.0690 & -0.0690 & -0.1964 & -0.2940 & -0.3468 & -0.3468 & -0.2940 & -0.1964 & -0.0690 & 0.0690 & 0.1964 & 0.2940 & 0.3468 \\ 0.3383 & 0.2243 & 0.0347 & -0.1667 & -0.3118 & -0.3519 & -0.2733 & -0.1026 & 0.1026 & 0.2733 & 0.3519 & 0.3118 & 0.1667 & -0.0347 & -0.2243 & -0.3383 \\ 0.3266 & 0.1353 & -0.1353 & -0.3266 & -0.3266 & -0.1353 & 0.1353 & 0.3266 & 0.3266 & 0.1353 & -0.1353 & -0.3266 & -0.3266 & -0.1353 & 0.1353 & 0.3266 \\ 0.3118 & 0.0347 & -0.2733 & -0.3383 & -0.1026 & 0.2243 & 0.3519 & 0.1667 & -0.1667 & -0.3519 & -0.2243 & 0.1026 & 0.3383 & 0.2733 & 0.0347 & -0.3118 \\ 0.2940 & -0.0690 & -0.3468 & -0.1964 & 0.1964 & 0.3468 & 0.0690 & -0.2940 & -0.2940 & 0.0690 & 0.3468 & 0.1964 & -0.1964 & -0.3468 & -0.0690 & 0.2940 \\ 0.2733 & -0.1667 & -0.3383 & 0.0347 & 0.3519 & 0.1026 & -0.3118 & -0.2243 & 0.2243 & 0.3118 & -0.1026 & -0.3519 & 0.0347 & 0.3383 & 0.1667 & -0.2733 \\ 0.25 & -0.25 & -0.25 & 0.25 & 0.25 & -0.25 & -0.25 & 0.25 & 0.25 & -0.25 & -0.25 & 0.25 & 0.25 & -0.25 & -0.25 & 0.25 \\ 0.2243 & -0.3118 & -0.1026 & 0.3519 & -0.0347 & -0.3383 & 0.1667 & 0.2733 & -0.2733 & -0.1667 & 0.3383 & 0.0387 & -0.3519 & 0.1026 & 0.3118 & -0.2243 \\ 0.1964 & -0.3468 & 0.0690 & 0.2940 & -0.2940 & -0.0690 & 0.3468 & -0.1960 & -0.1960 & 0.3468 & -0.0690 & -0.2940 & 0.2940 & 0.0690 & -0.3468 & 0.1964 \\ 0.1667 & -0.3519 & 0.2243 & 0.1026 & -0.3383 & 0.2733 & 0.0347 & -0.3118 & 0.3118 & 0.0347 & -0.2733 & 0.3383 & -0.1026 & -0.2243 & 0.3519 & -0.1667 \\ 0.1353 & -0.3266 & 0.3266 & -0.1353 & -0.1353 & 0.3266 & -0.3266 & 0.1353 & 0.1353 & -0.3266 & 0.3266 & -0.1353 & -0.1353 & 0.3266 & -0.3266 & 0.1353 \\ 0.1026 & -0.2733 & 0.3519 & -0.3118 & 0.1667 & 0.0347 & -0.2243 & 0.3383 & -0.3383 & 0.2243 & -0.0347 & -0.1667 & 0.3118 & -0.3519 & 0.2733 & -0.1026 \\ 0.0696 & -0.1964 & 0.2940 & -0.3468 & 0.3468 & -0.2940 & 0.1964 & -0.0690 & -0.0690 & 0.1964 & -0.2940 & 0.3468 & -0.3468 & 0.2940 & -0.1964 & 0.0690 \\ 0.0347 & -0.1026 & 0.1667 & -0.2243 & 0.2733 & -0.3118 & 0.3383 & -0.3519 & 0.3519 & -0.3383 & 0.3118 & -0.2733 & 0.2243 & -0.1667 & 0.1026 & -0.0347 \end{bmatrix}. \quad (16)$$

The ZP-MMSE equalizer is given as:

$$\mathbf{G} = E_s (E_s \mathbf{H}_0^H \mathbf{H}_0 + \sigma_v^2 \mathbf{I}_M)^{-1} \mathbf{H}_0^H. \quad (22)$$

In (22), $E_s = E[X_k^2]$ is the signal power per symbol, σ_v^2 is the AWGN noise power, $(\cdot)^H$ denotes the Hermitian operator. The equalized signal at the receiver side after removing the ZP can be written as

$$\begin{aligned} \mathbf{y}_{eq} &= \mathbf{L}_{zp}^H \mathbf{G} \mathbf{y}, \\ &= \mathbf{L}_{zp}^H \mathbf{G} \mathbf{H}_0 \mathbf{u} + \mathbf{L}_{zp}^H \mathbf{G} \mathbf{v}. \end{aligned} \quad (23)$$

At the receiver side, the received data \mathbf{y}_{eq} is first processed by the C-transform as follows

$$\begin{aligned} \hat{\mathbf{X}} &= \mathbf{C} \mathbf{L}_{zp}^H \mathbf{G} \mathbf{H}_0 \mathbf{L}_{zp} \mathbf{x} + \mathbf{C} \mathbf{L}_{zp}^H \mathbf{G} \mathbf{v}, \\ &= \mathbf{C} \mathbf{L}_{zp}^H \mathbf{G} \mathbf{H}_0 \mathbf{L}_{zp} \mathbf{C}^T \mathbf{X} + \mathbf{C} \mathbf{L}_{zp}^H \mathbf{G} \mathbf{v}. \end{aligned} \quad (24)$$

The noise signal, $\mathbf{e} = \hat{\mathbf{X}} - \mathbf{X}$, is then given as

$$\mathbf{e} = (\mathbf{C} \mathbf{L}_{zp}^H \mathbf{G} \mathbf{H}_0 \mathbf{L}_{zp} \mathbf{C}^T - \mathbf{I}_N) \mathbf{X} + \mathbf{C} \mathbf{L}_{zp}^H \mathbf{G} \mathbf{v}. \quad (25)$$

In order to calculate the received signal power and the noise power, (24) and (25) need to be simplified. This simplification should start with the equalizer matrix \mathbf{G} . The \mathbf{G} matrix can be factorized using singular value decomposition (SVD) algorithm by simplifying its contents. The channel matrix, \mathbf{H}_0 , can be factorized to $\mathbf{W} \mathbf{\Sigma} \mathbf{V}^H$, consequently, \mathbf{H}_0^H is equivalent to $\mathbf{V} \mathbf{\Sigma}^H \mathbf{W}^H$, where $\mathbf{\Sigma}$ is a diagonal matrix, its diagonal elements are the square roots of the eigenvalues of $\mathbf{H}_0^H \mathbf{H}_0$ arranged in a descending order, \mathbf{V} is a matrix with columns equal to eigenvectors of $\mathbf{H}_0^H \mathbf{H}_0$ while the columns of \mathbf{W} are the eigenvectors of $\mathbf{H}_0 \mathbf{H}_0^H$. Then \mathbf{G} in (22) can be rewritten as

$$\mathbf{G} = E_s (E_s \mathbf{V} \mathbf{\Sigma}^H \mathbf{\Sigma} \mathbf{V}^H + \sigma_v^2 \mathbf{I}_M)^{-1} \mathbf{V} \mathbf{\Sigma}^H \mathbf{W}^H. \quad (26)$$

Using $(\mathbf{A} \mathbf{B})^{-1} = \mathbf{B}^{-1} \mathbf{A}^{-1}$, (26) can be rewritten as

$$\begin{aligned} \mathbf{G} &= E_s \{ (\mathbf{V} \mathbf{\Sigma}^H)^{-1} (E_s \mathbf{V} \mathbf{\Sigma}^H \mathbf{\Sigma} \mathbf{V}^H + \sigma_v^2 \mathbf{I}_M) \}^{-1} \mathbf{W}^H, \\ &= E_s \{ E_s \mathbf{\Sigma} \mathbf{V}^H + (\mathbf{V} \mathbf{\Sigma}^H)^{-1} \sigma_v^2 \mathbf{I}_M \}^{-1} \mathbf{W}^H. \end{aligned} \quad (27)$$

Using the fact that $\mathbf{V}^H = \mathbf{V}^{-1}$, the first term of (27) can be written in more expressive way as:

$$\begin{aligned} \mathbf{\Sigma} \mathbf{V}^H &= \mathbf{\Sigma} (\mathbf{\Sigma}^H \mathbf{\Sigma}^H)^{-1} \mathbf{V}^{-1}, \\ &= \mathbf{\Sigma} \mathbf{\Sigma}^H (\mathbf{V} \mathbf{\Sigma}^H)^{-1}. \end{aligned} \quad (28)$$

Substituting (28) into (27), \mathbf{G} can be simplified to

$$\begin{aligned} \mathbf{G} &= E_s \{ E_s \mathbf{\Sigma} \mathbf{\Sigma}^H (\mathbf{V} \mathbf{\Sigma}^H)^{-1} + \sigma_v^2 \mathbf{I}_M (\mathbf{V} \mathbf{\Sigma}^H)^{-1} \}^{-1} \mathbf{W}^H, \\ &= E_s \mathbf{V} \mathbf{\Sigma}^H (E_s \mathbf{\Sigma} \mathbf{\Sigma}^H + \sigma_v^2 \mathbf{I}_M)^{-1} \mathbf{W}^H. \end{aligned} \quad (29)$$

Substituting (29) into (25) yield

$$\begin{aligned} \mathbf{e} &= \left[E_s \mathbf{C} \mathbf{L}_{zp}^H \mathbf{V} \mathbf{\Sigma}^H (E_s \mathbf{\Sigma} \mathbf{\Sigma}^H + \sigma_v^2 \mathbf{I}_M)^{-1} \right. \\ &\quad \times \mathbf{W}^H (\mathbf{W} \mathbf{\Sigma} \mathbf{V}^H) \mathbf{L}_{zp} \mathbf{C}^T - \mathbf{I}_N \left. \right] \mathbf{X} \\ &\quad + E_s \mathbf{C} \mathbf{L}_{zp}^H \mathbf{V} \mathbf{\Sigma}^H (E_s \mathbf{\Sigma} \mathbf{\Sigma}^H + \sigma_v^2 \mathbf{I}_M)^{-1} \mathbf{W}^H \mathbf{v}. \end{aligned} \quad (30)$$

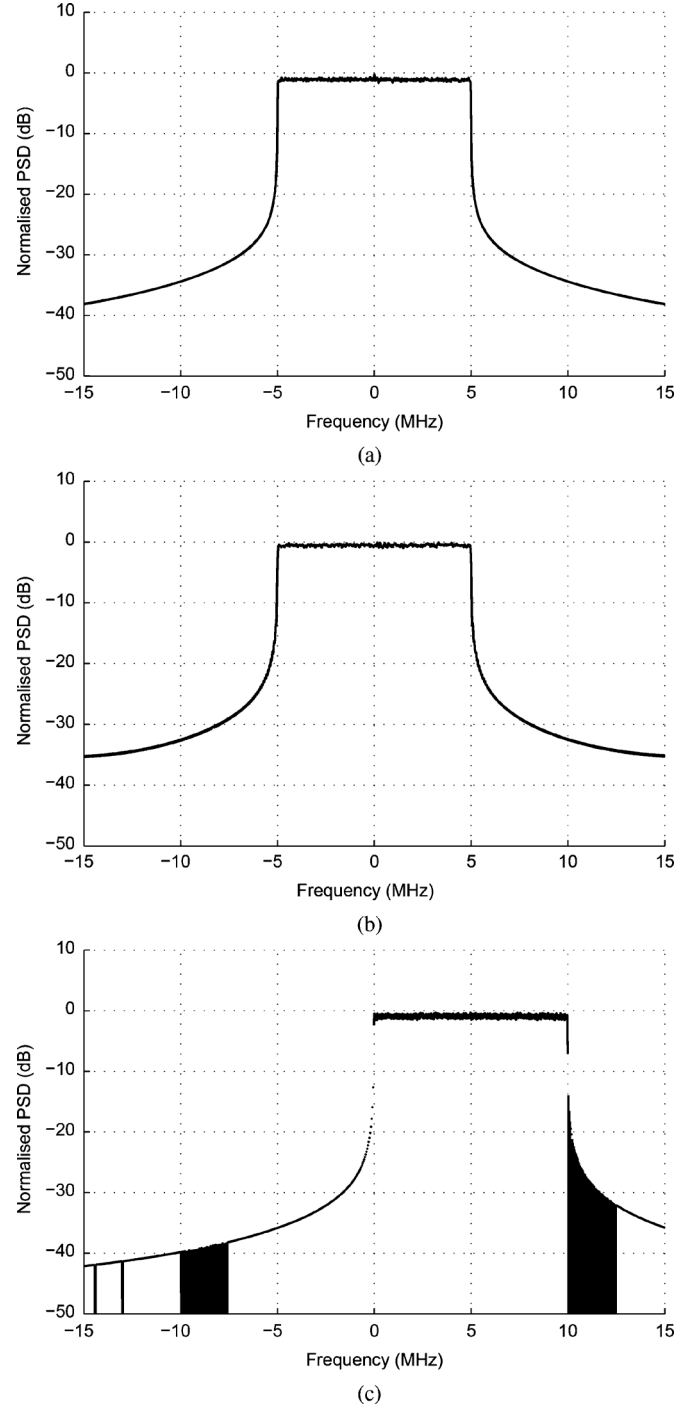


Fig. 3. Power spectral densities of DCT, CT and DFT based OFDM systems. (a) Power spectral density of DCT-OFDM systems, (b) Power spectral density of C-OFDM systems, (c) Power spectral density of DFT-OFDM system.

Since, \mathbf{C} is a real transform, then $\mathbf{C}^T = \mathbf{C}^H$ and let $\mathbf{\Delta}_{N \times M}$ represents the combination $\mathbf{C} \mathbf{L}_{zp}^H \mathbf{V}$. For simplicity, $\mathbf{\Delta}_{N \times M}$ will be written as $\mathbf{\Delta}$ only without the subscript, after some algebra, (30) can be rewritten as

$$\begin{aligned} \mathbf{e} &= \left[E_s \mathbf{\Delta} \mathbf{\Sigma}^H (E_s \mathbf{\Sigma} \mathbf{\Sigma}^H + \sigma_v^2 \mathbf{I}_M)^{-1} \mathbf{\Sigma} \mathbf{\Delta}^H - \mathbf{I}_N \right] \mathbf{X} \\ &\quad + E_s \mathbf{\Delta} \mathbf{\Sigma}^H (E_s \mathbf{\Sigma} \mathbf{\Sigma}^H + \sigma_v^2 \mathbf{I}_M)^{-1} \mathbf{W}^H \mathbf{v}. \end{aligned} \quad (31)$$

The above equation can be rewritten as

$$\mathbf{e} = \Delta \left[E_s \Sigma^H (E_s \Sigma \Sigma^H + \sigma_v^2 \mathbf{I}_M)^{-1} \Sigma - \mathbf{I}_M \right] \Delta^H \mathbf{X} + E_s \Delta \Sigma^H (E_s \Sigma \Sigma^H + \sigma_v^2 \mathbf{I}_M)^{-1} \mathbf{W}^H \mathbf{v}. \quad (32)$$

In (32), $[E_s \Sigma^H (E_s \Sigma \Sigma^H + \sigma_v^2 \mathbf{I}_M)^{-1} \Sigma] = \Theta_1$, $[E_s \Sigma^H (E_s \Sigma \Sigma^H + \sigma_v^2 \mathbf{I}_M)^{-1} \Sigma - \mathbf{I}_M] = \Theta_2$ and $E_s \Sigma^H (E_s \Sigma \Sigma^H + \sigma_v^2 \mathbf{I}_M)^{-1} = \Theta_3$ where Θ_1 , Θ_2 and Θ_3 are diagonal matrices with their i_{th} diagonal entries are respectively given as

$$[\Theta_1]^{i,i} = \frac{E_s |\lambda_i|^2}{E_s |\lambda_i|^2 + \sigma_v^2}, \quad (33)$$

$$= \frac{\gamma_s |\lambda_i|^2}{\gamma_s |\lambda_i|^2 + 1},$$

$$[\Theta_2]^{i,i} = \frac{-\sigma_v^2}{E_s |\lambda_i|^2 + \sigma_v^2}, \quad (34)$$

$$= \frac{-1}{\gamma_s |\lambda_i|^2 + 1},$$

$$[\Theta_3]^{i,i} = \frac{E_s |\lambda_i|}{E_s |\lambda_i|^2 + \sigma_v^2}, \quad (35)$$

$$= \frac{\gamma_s |\lambda_i|}{\gamma_s |\lambda_i|^2 + 1},$$

where λ_i , ($i = 0, 1, 2, \dots, M-1$) is the i_{th} element of the diagonal of Σ and $\gamma_s = \frac{E_s}{\sigma_v^2}$ is the signal power (per symbol)-to-noise ratio. Therefore, (32) can be rewritten as

$$\mathbf{e} = \Delta \Theta_2 \Delta^H \mathbf{X} + \Delta \Theta_3 \mathbf{W}^H \mathbf{v}. \quad (36)$$

Similarly, $\hat{\mathbf{X}}$ in (24) can be written as

$$\hat{\mathbf{X}} = \Delta \Theta_1 \Delta^H \mathbf{X} + \Delta \Theta_3 \mathbf{W}^H \mathbf{v}. \quad (37)$$

The total noise power at the receiver side is $\mathcal{P}_n = E[\mathbf{e}\mathbf{e}^H] = \text{tr}(\mathbf{e}\mathbf{e}^H)$ and is given as

$$\mathcal{P}_n = \text{tr} [\Delta E_s \Theta_2^2 \Delta^H + \Delta \sigma_v^2 \Theta_3^2 \Delta^H], \quad (38)$$

$$= \text{tr} [\Delta (E_s \Theta_2^2 + \sigma_v^2 \Theta_3^2) \Delta^H].$$

In (38), $[E_s \Theta_2^2 + \sigma_v^2 \Theta_3^2]$ is a diagonal matrix which can be simplified as

$$[E_s \Theta_2^2 + \sigma_v^2 \Theta_3^2]_{i,i} = \frac{E_s}{[\gamma_s |\lambda_i|^2 + 1]^2} + \frac{\sigma_v^2 \gamma_s^2 |\lambda_i|^2}{[\gamma_s |\lambda_i|^2 + 1]^2}, \quad (39)$$

$$= \frac{E_s}{[\gamma_s |\lambda_i|^2 + 1]^2} + \frac{E_s \gamma_s |\lambda_i|^2}{[\gamma_s |\lambda_i|^2 + 1]^2},$$

$$= \frac{E_s}{\gamma_s |\lambda_i|^2 + 1}.$$

Let $\Theta_4 = \text{diag}(\frac{1}{\gamma_s |\lambda_i|^2 + 1})$ and by substituting (39) into (38) yields

$$\mathcal{P}_n = \text{tr} [\Delta E_s \Theta_4 \Delta^H]. \quad (40)$$

The total power of the received signal is $\mathcal{P}_s = E[\hat{\mathbf{X}}\hat{\mathbf{X}}^H] = \text{tr}(\hat{\mathbf{X}}\hat{\mathbf{X}}^H)$ is given as

$$\mathcal{P}_s = \text{tr} [\Delta E_s \Theta_1^2 \Delta^H + \Delta \sigma_v^2 \Theta_3^2 \Delta^H], \quad (41)$$

$$= \text{tr} [\Delta (E_s \Theta_1^2 + \sigma_v^2 \Theta_3^2) \Delta^H],$$

$$= \text{tr} [\Delta E_s \Theta_1 \Delta^H].$$

Therefore, the signal-to-noise ratio at the output of the m_{th} subchannel is given as

$$\text{SNR}_m = \frac{[\Delta \Theta_1 \Delta^H]_{m,m}}{[\Delta \Theta_4 \Delta^H]_{m,m}}. \quad (42)$$

The overall BER can be given by averaging the BER for the individual subchannels [29] as follows

$$P_e^{M-PSK} = \frac{\mu}{m_b} \frac{1}{N} \sum_{m=0}^{N-1} Q \left(\sqrt{2\text{SNR}_m} \sin \left(\frac{\pi}{M_l} \right) \right), \quad (43)$$

$$P_e^{M-QAM} = \frac{4 - 2^{(2-m_b/2)}}{m_b} \frac{1}{N} \sum_{m=0}^{N-1} Q \left(\sqrt{\frac{3\text{SNR}_m}{M_l - 1}} \right). \quad (44)$$

In (43) and (44), μ denotes the number of nearest neighbors signal points ($\mu_{\text{QPSK}} = 2$ and $\mu_{16\text{-QAM}} = 3$), M_l is the level on constellation and $m_b = \log_2 M_l$ represents the number of bits in each digitally encoded symbol, $Q(x)$ denotes the Q-function of x and SNR_m is the signal power, per symbol, to noise power ratio. In other words, by substituting the specific parameters that assigned to QPSK and 16-QAM, the BER is respectively given as

$$P_e^{\text{QPSK}} = \frac{1}{N} \sum_{m=0}^{N-1} Q \left(\sqrt{\frac{[\Delta \Theta_1 \Delta^H]_{m,m}}{[\Delta \Theta_4 \Delta^H]_{m,m}}} \right), \quad (45)$$

$$P_e^{16\text{-QAM}} = \frac{3}{4N} \sum_{m=0}^{N-1} Q \left(\sqrt{\frac{[\Delta \Theta_1 \Delta^H]_{m,m}}{5[\Delta \Theta_4 \Delta^H]_{m,m}}} \right). \quad (46)$$

The advantages of employing the **C**-transform in the OFDM can be attributed to the fact that the **C**-transform further distributes the information symbols among the channel spectrum mitigating the effect of narrowband notches of the channel spectral as the data symbol on significantly attenuated subcarrier is not completely disappeared where it can be recovered from the other unaffected subcarriers.

It is noteworthy that the SNR approach in (42) is a general formula describing the BER performance of ZP-OFDM with MMSE detection and can be applied to attain the BER performance for the DCT-OFDM or the DFT-OFDM simply by replacing the **C** transform by either the DCT or the DFT respectively.

Finally, the recovered transmitted bits are obtained by applying the demodulation process on the recovered complex modulated data symbols $\hat{\mathbf{X}}$.

IV. PAPR ANALYSIS AND SSPA DISTORTION

The PAPR in the transmitted signal of the OFDM systems is considered as one of the main problems plaguing the OFDM systems [30], which arises from the superposition of a large number of symbols.

In general, the PAPR for a given OFDM block can be written as

$$\text{PAPR}\{x_k\} = \frac{\max_{0 \leq k \leq N-1} |x_k|^2}{E[|x_k|^2]}, \quad (47)$$

where $\max_{0 \leq k \leq N-1}$ denotes the maximum instantaneous power and $E[|x_k|^2]$ denotes the average power of the signal. Hence, the PAPR for the case of the C-OFDM system can be upper bounded as

$$\text{PAPR}\{x_k\} < \frac{N |X_n|_{\max}^2}{2 E[|X_n|^2]}. \quad (48)$$

This is because the C-transform has a block diagonal structure with two-third of its element being zero as shown in (15). Thus each of N output samples from ICT operation involves less than or equal to the sum of $\frac{N}{2}$ symbols. In contrast, for the case of the DCT-OFDM or DFT-OFDM, each output sample involves the superposition of N input symbols. Therefore, their PAPR can be upper bounded as

$$\begin{aligned} x_k^{\text{DCT-OFDM}} &= \sqrt{\frac{2}{N}} \sum_{m=0}^{N-1} X_m \kappa_m \cos\left(\frac{\pi(2k+1)m}{2N}\right) \\ x_k^{\text{DFT-OFDM}} &= \frac{1}{\sqrt{N}} \sum_{m=0}^{N-1} X_m e^{j\frac{2\pi km}{N}}. \end{aligned} \quad (49)$$

Then $\max_{0 \leq k \leq N-1} |x_k|^2 \leq N |X_m|_{\max}^2$, and $E[|x_k|^2] = E[|X_m|^2]$, $0 \leq k \leq N-1$, Hence the PAPR can be upper bounded as

$$\text{PAPR}\{x_k\} \leq N \frac{|X_m|_{\max}^2}{E[|X_m|^2]}. \quad (50)$$

In (50), equality is attained at $k = 0$ where all the sub-symbols have the same phase. In particular, each of the N output samples from the IDCT or the IFFT operation involves the sum of N symbols.

The worst case of the PAPR is of order N for the DFT-OFDM and DCT-OFDM whilst it is of order $\frac{N}{2}$ for the proposed C-OFDM system.

$$\begin{aligned} &(\text{PAPR}_{\text{C-OFDM}_{\max}})_{\text{dB}} \\ &< (\text{PAPR}_{\text{DCT-OFDM}_{\max}} - 3)_{\text{dB}} \\ &< (\text{PAPR}_{\text{DFT-OFDM}_{\max}} - 3)_{\text{dB}} \end{aligned} \quad (51)$$

Our simulation results showed 1 dB improvement in complementary cumulative distribution function (CCDF) for the case of the proposed C-OFDM system in comparison with that for the DCT-OFDM or the DFT-OFDM systems.

The non-linear distortion arising from clippings in the transmitted signal due to the SSPA has a detrimental effect on the

OFDM performance. Therefore, further investigation into the BER performance of the proposed approach when the system encompasses SSPA power amplifier within its structure is presented in this section. Let us define the IBO, the operating point of the SSPA power amplifier, as $\text{IBO} = 10 \log_{10} \frac{P_{\text{in,max}}}{P_{\text{in,av}}}$, where $P_{\text{in,max}}$ and $P_{\text{in,av}}$ denote the maximum (saturation) and the average powers of the amplifier input respectively. The complex envelope on the continuous version of the transmitted signal, u , can be written as

$$u(t) = \rho(t)e^{j\theta(t)}, \quad (52)$$

where $\rho(t)$ and $\theta(t)$ respectively represent the amplitude and the phase of the signal $u(t)$. The amplified signal is given as $s_k = u_k G_a[|u_k|]$, where $G_a[|u_k|]$ is the amplifier gain and it is given as

$$G_a[|u_k|] = \frac{A_m[|u_k|] e^{j\phi[|u_k|]}}{|u_k|}, \quad (53)$$

where $\phi[|u_k|]$ represents the amplitude modulation/phase modulation AM/PM conversion of the non-linear power amplifier and $A_m[|u_k|]$ represents the amplitude modulation/amplitude modulation AM/AM conversion of the non-linear power amplifier which is given as [31]

$$A_m[|u_k|] = \frac{|u_k|}{\left[1 + \left(\frac{|u_k|}{A_s}\right)^{2p}\right]^{\frac{1}{2p}}}. \quad (54)$$

In (54), A_s is the amplifier input saturation voltage and p is a parameter which controls the transition smoothness from the linear region to the saturation region. Equation (54) reveals that for an SSPA with a small IBO, A_s is small (low saturation level), this, in turn, leads to amplitude clippings and ultimately BER performance degradation.

V. COMPUTATIONAL COMPLEXITY ANALYSIS

In this section, the arithmetic complexity of the C-transform is analyzed and compared with the DCT, WHT-DCT and FFT transforms. For fair comparison, all calculations are based on radix-2 single butterfly algorithms.

It is worth mentioning that our true comparison is with DCT and WHT-DCT, however, comparison with FFT transforms is added for further information.

A. C Transform

As shown in (12), the C-transform has a block-diagonal-structure (BDS) with more than 2/3 of its matrix elements being zero; hence, its direct computation will only involve $N^2/3$ real multiplications and $N(N-1)/3$ real additions. However, when fast algorithm is applied, this can be reduced even further. In general, the radix-2 fast algorithm for the C-transform involves a number of butterflies given as:

$$\text{Butt}_{\text{flies}} = \frac{N}{2} \log_2 N - N + 1. \quad (55)$$

TABLE I
COMPARISON OF REAL ARITHMETIC OPERATIONS FOR THE PROPOSED C TRANSFORM, DCT, WHT-DCT AND
FFT TRANSFORMS UNDER COMPLEX CONSTELLATION CONSIDERATION

N	CT			DCT			WHT-DCT			FFT		
	R_A	R_M	R_O	R_A	R_M	R_O	R_A	R_M	R_O	R_A	R_M	R_O
32	294	294	588	320	160	480	640	160	800	480	320	800
64	774	774	1548	768	384	1152	1536	384	1920	1152	768	1920
128	1926	1926	3852	1792	896	2688	3584	896	4480	2688	1792	4480
256	4614	4614	9228	4096	2048	6144	8192	2048	10240	6144	4096	10240
512	10758	10758	21516	9216	4608	13824	18432	4608	23040	13824	9216	23040
1024	24582	24582	49164	20480	10240	30720	40960	10240	51200	30720	20480	51200
2048	55302	55302	110604	45056	22528	67584	90112	22528	112640	67584	45056	112640
4096	122886	122886	245772	98304	49152	147456	196608	49152	245760	147456	98304	245760

Each butterfly involves 3 real multiplications (R_M) and 3 real additions (R_A). Thus the complexity of the C-transform involves $R_M = \frac{3}{2}N \log_2 N - 3N + 3$ and $R_A = \frac{3}{2}N \log_2 N - 3N + 3$ and then the total number of real operations (R_O) is given as

$$R_O = 3N \log_2 N - 6N + 6. \quad (56)$$

It is worth mentioning that, for the case of complex constellation, the arithmetic operations of C transform that is given in (56) must be calculated twice, one for the real part and the other for the imaginary part, and the overall complexity is given as

$$R_O = 6N \log_2 N - 12N + 12. \quad (57)$$

B. Discrete Cosine Transform (DCT)

The arithmetic complexity of fast implementation of DCT based on single butterfly algorithm can be given as [32]: Number of real multiplications $R_M = \frac{N}{2} \log_2 N$ and number of real additions $R_A = N \log_2 N$ thus the total number of real operation is given as $R_O = \frac{3N}{2} \log_2 N$. It is worth mentioning that when complex constellation is used, the complexity above should be calculated twice (one for real part of the signal while the other for the imaginary part) and the arithmetic complexity will be equal to $R_O = 3N \log_2 N$

C. WHT-DCT

The arithmetic complexity of fast implementation of the WHT followed by the DCT can be given as: The WHT complexity includes just $R_A = N \log_2 N$ real additions while the arithmetic operations of the radix-2 DCT using single butterfly algorithm is given above as: $R_M = \frac{N}{2} \log_2 N$ and $R_A = N \log_2 N$ for real multiplications and additions respectively. Then the total number of real multiplications and additions for the WHT-DCT is given by

$$R_O = \frac{5N}{2} \log_2 N. \quad (58)$$

Same as for the case of C-transform, when complex constellation is used, (58) must be calculated twice and the arithmetic complexity will be given as

$$R_O(\text{WHT-DCT}) = 5N \log_2 N. \quad (59)$$

D. Fast Fourier Transform (FFT)

In this section we will consider complex FFT only, each FFT of order N involves: $C_M = \frac{N}{2} \log_2 N$ complex multiplications and $C_A = N \log_2 N$ complex additions. By rendering the fact that each complex multiplication is equal to 4 real multiplications and 2 real additions and each complex addition is equal to 2 real additions; that is radix-2 FFT based on single butterfly algorithm involves $R_M = 2N \log_2 N$ and $R_A = 3N \log_2 N$, hence, R_O is equal to $5N \log_2 N$.

Table I shows the computational complexity for the C-transform, DCT, WHT-DCT and FFT for different transform lengths N when complex constellation is considered (all the C-transform, DCT and the WHT-DCT are used twice, one for the real part of the complex data while the other for the imaginary part).

E. Receiver Complexity

The MMSE receivers of the C-OFDM, DCT-OFDM and DFT-OFDM with zero-padding have the same degree of complexity. The equalizer complexity of the C-OFDM and DCT-OFDM with zero-padding is higher than the complexity of the DFT-OFDM equalizer with a cyclic prefix [22] in the case of a quasi-static channel where the channel equalization could be done in the frequency domain by simple one tap equalizer. However, the ZP-C-OFDM, ZP-DCT-OFDM, ZP-DFT-OFDM and CP-DFT-OFDM have the same equaliser complexity if they are used over fast fading environment where the channel equalization needs to be carried out in the time-domain. In this work, the ITU pedestrian B and vehicular A channel models, which varies among the OFDM transmission while it is constant during each single OFDM symbol, is adopted in this work.

The main complexity of the MMSE receiver comes from the calculation of $\mathbf{H}_0^H (\mathbf{H}_0 + \sigma_v^2 \mathbf{I}_M)^{-1} \mathbf{H}_0^H$. The number of operations in the above MMSE equation can be calculated using several algorithms [33]. The method of normal equation, for instance, gives a computational complexity of $7N^3/3 + N^2 L_G$. As N is the number of subcarriers in single OFDM symbol, the per-symbol complexity is then given as $7N^2/3 + N L_G$.

VI. SIMULATION RESULTS AND DISCUSSION

In this section, results are elaborated to demonstrate the performance of the proposed C-OFDM and compare it with that of the DCT-OFDM and DFT-OFDM systems. It should be noted that the true comparison should be with the DCT-OFDM as both

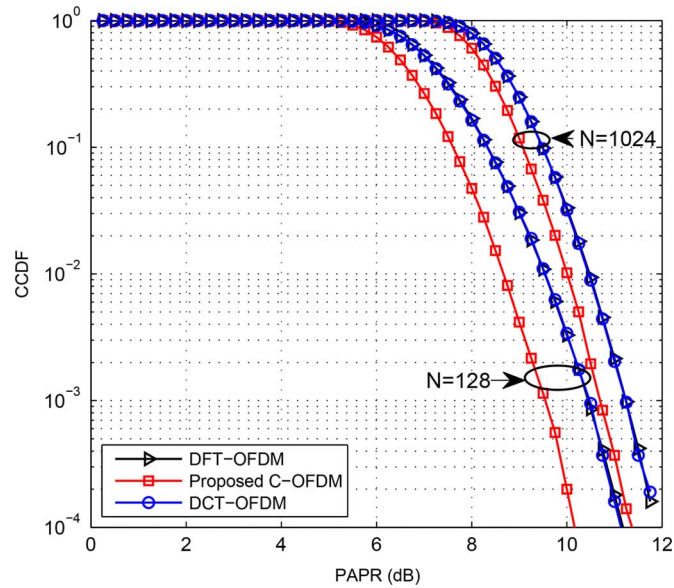


Fig. 4. PAPR performance of the proposed C-OFDM, DCT-OFDM and DFT-OFDM systems using 16-QAM modulation format, the DCT-OFDM and DFT-OFDM systems have the same graphs.

the C-transform and the DCT are real transforms. However, we added the comparison with the DFT-OFDM for more information.

A. PAPR Reduction

A simulation was carried out for the C-OFDM, DFT-OFDM and DCT-OFDM systems, showing that the C-OFDM has the lowest PAPR for different number of subcarriers ($N = 128$, and 1024) and 16-QAM modulation formats. In order to have an awareness and intuitive view of the PAPR statistics, complementary cumulative density function (CCDF) was plotted. Also to ensure the reliability of computer simulations, 10^5 OFDM symbols were generated to obtain each PAPR value. It is noted from Fig. 4 that the C-OFDM system has a better PAPR than the DCT-OFDM and DFT-OFDM for different numbers of subcarriers. Fig. 4 also shows that the DCT-OFDM system achieves the same PAPR as the DFT-OFDM while the proposed C-OFDM achieved about 1 dB improvement at a CCDF of 10^{-4} . This is due to the fact that the C transform has a block-diagonal-structure that reduces the superposition of the input symbols involved in the calculation of each OFDM sample. This phenomenon, however, does not exist in the DCT-OFDM or DFT-OFDM systems counterpart shown in (12)–(16).

B. BER Performance

1) *BER Performance Over AWGN Channel:* The BER performance of the C-OFDM, DCT-OFDM and DFT-OFDM systems over AWGN channel for 16-QAM modulation format is shown in Fig. 5. It reveals that all of these systems have the same BER performance over the AWGN channel because the AWGN noise power is distributed equally (white noise) among all the subchannels, so there are no channel dips. This in turn,

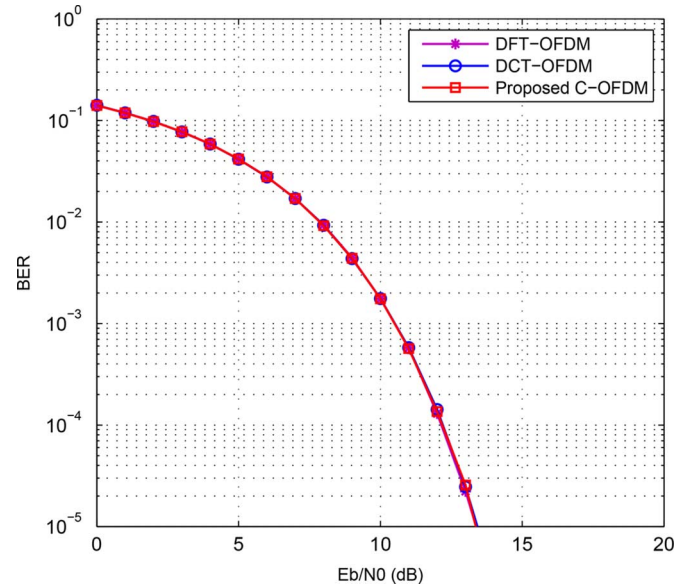


Fig. 5. BER performance of the proposed C-OFDM, DCT-OFDM and DFT-OFDM systems over AWGN channel model for 16-QAM modulation format. All have the same graphs.

illustrates that the C-transform preserves the orthogonality in exactly the same way as the DCT and FFT transforms where all the data are equally recovered. However, the superiority of the C-OFDM in terms of the BER performance is pronounced over multipath fading channels showing high signal diversity and achieving significant performance gain over the DFT-OFDM and DCT-OFDM systems as shown in the next section.

2) *BER Performance Over Multipath Channel:* Besides the PAPR reduction, channel diversity exploitation is another advantage of adopting the C transform in OFDM systems which is pronounced over multipath frequency selective channels. To illustrate this advantage, ITU pedestrian B and vehicular A channel models according to the WiMAX standard and the ZP-MMSE detection were utilized in this work; where the following parameters were used: The transmission bandwidth is 10 MHz, the carrier frequency is 4 GHz and number of subcarriers $N = 1024$, the guard length $L_G = 256$. Since the channel length is shorter than the guard length, no ISI occurs in our simulations. In the case of the DCT-OFDM and DFT-OFDM systems, the ICT/CT in Fig. 2 are replaced by the cosine transform matrix (IDCT/DCT) or Fourier transform matrix (IDFT/DFT) respectively. Two signal constellations, QPSK and 16-QAM, were adopted in this work.

It can be seen from Figs. 6 and 7 that the theoretical results are in strong accordance with those simulated by computer, illustrating that the proposed C-OFDM significantly outperforms both the DCT-OFDM and the DFT-OFDM systems under; pedestrian B and vehicular A channel models, perfect channel state information CSI assumption, and for QPSK and 16-QAM modulation formats.

Fig. 6 shows the BER performance of the ZP-C-OFDM, ZP-DCT-OFDM and ZP-DFT-OFDM systems over the ITU class B pedestrian channel and for 16-QAM and QPSK

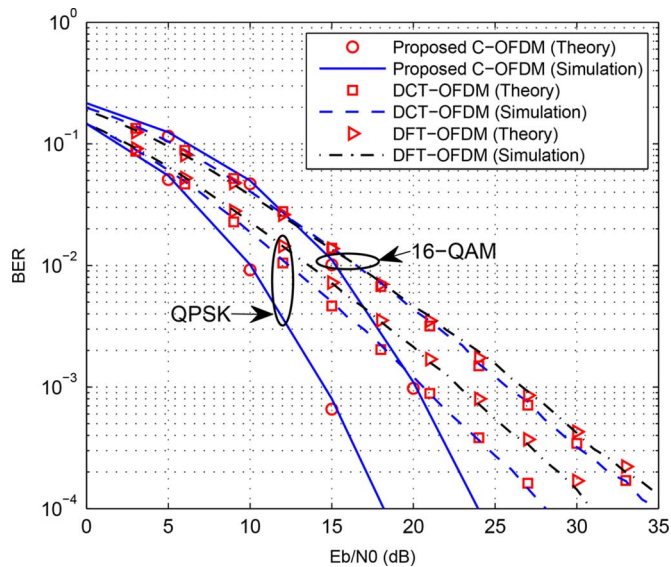


Fig. 6. BER performance of the proposed C-OFDM, DCT-OFDM and DFT-OFDM systems over ITU pedestrian B channel for QPSK and 16-QAM modulation formats.

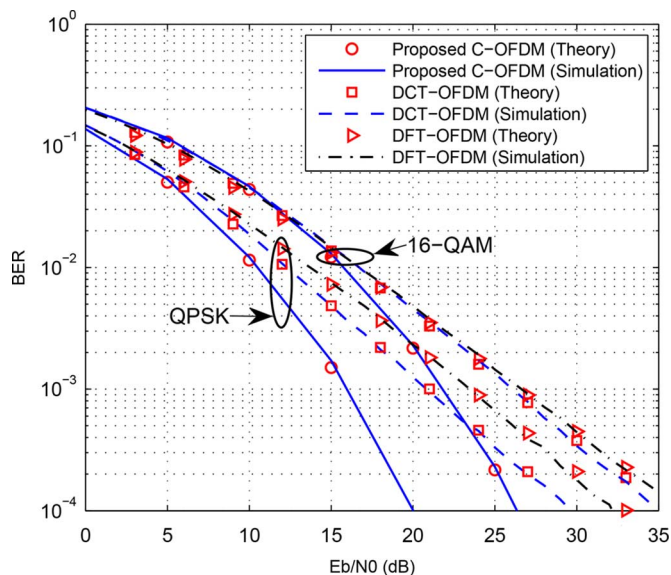


Fig. 7. BER performance of the proposed C-OFDM, DCT-OFDM and DFT-OFDM systems over ITU vehicular A channel model for QPSK and 16-QAM modulation formats.

modulation formats. It is evident that at 10^{-4} BER, the proposed C-OFDM achieves about 10 dB E_b/N_0 gain over the ZP-DCT-OFDM and ZP-DFT-OFDM. This can be attributed to the fact that the C-transform has a block diagonal structure that is less affected by multipath channels which leads to this high gain in E_b/N_0 . On the contrary, this gain is not achievable by the DCT-OFDM as the information symbol on deep notch subchannel can not be recovered at the transmitter from other unaffected subcarriers.

Over a vehicular A channel, it can be seen from Fig. 7 that, for QPSK and 16-QAM modulation formats, the C-OFDM scheme still retains the valuable BER improvement in comparison with DCT-OFDM and DFT-OFDM ones.

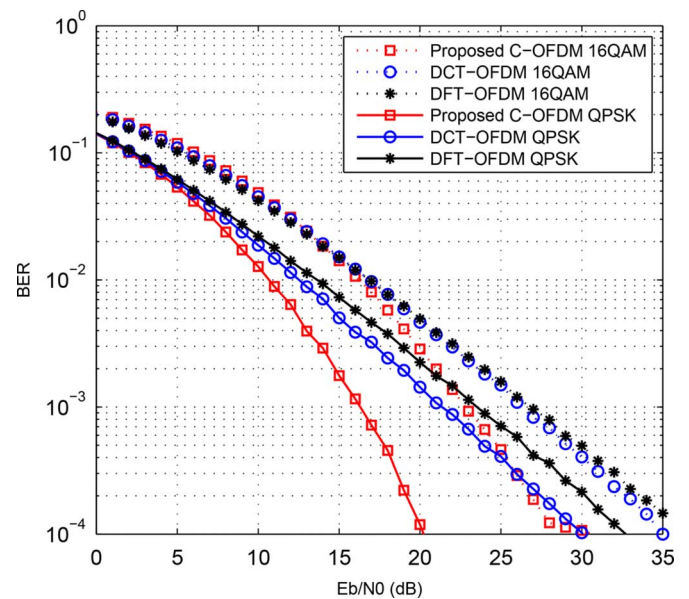


Fig. 8. BER performance of the proposed C-OFDM, DCT-OFDM and DFT-OFDM systems of QPSK and 16-QAM modulation formats with SSPA (IBO = 7 dB) over ITU Vehicular A channel model.

3) *BER Performance in the Presence of SSPA:* In this section, we further investigate the BER performance of the proposed scheme in the presence of the SSPA high power amplifier. For the QPSK and 16-QAM modulation formats and 8 dB input back-off (IBO), Fig. 8 shows the BER performance of the proposed scheme, the DCT-OFDM and DFT-OFDM systems under the ITU vehicular A channel model.

It is clear from Fig. 8 that at 10^{-4} BER, for QPSK constellation, the proposed scheme still retains the same E_b/N_0 gain. However, this gain is reduced to around 6 dB for the case of 16-QAM constellation format.

4) *BER Performance in the Presence of CFO:* The BER performance in the presence of CFO of the proposed C-OFDM system compared with those of DCT-OFDM and DFT-OFDM systems is investigated in this subsection. Fig. 9 shows the BER performance of the proposed OFDM, DCT-OFDM and DFT-OFDM systems for different values of the normalized CFO ϵ ($\epsilon = 0.03, 0.06$ and 0.1). It is evident that the proposed system surpasses the DCT-OFDM and DFT-OFDM systems for small ϵ around 0.03 whereas it has less BER performance for ϵ around 0.06. However, it is also evident that all of the aforementioned systems will completely lose their orthogonality when ϵ is above 0.1. The proposed C-OFDM system is slightly more sensitive to the CFO than both DCT-OFDM and the conventional OFDM systems when no synchronization algorithm is applied. This is because any shift in subcarrier frequency will be spread over others by the C-transform. However, all the DCT-OFDM, the conventional OFDM and the C-OFDM systems completely lose their orthogonality when CFO, normalized to the subcarrier spacing, is larger than or equal to 0.1. The C-OFDM system restore its superiority over the others when a CFO synchronization algorithm is used. The range of applications of the proposed scheme can

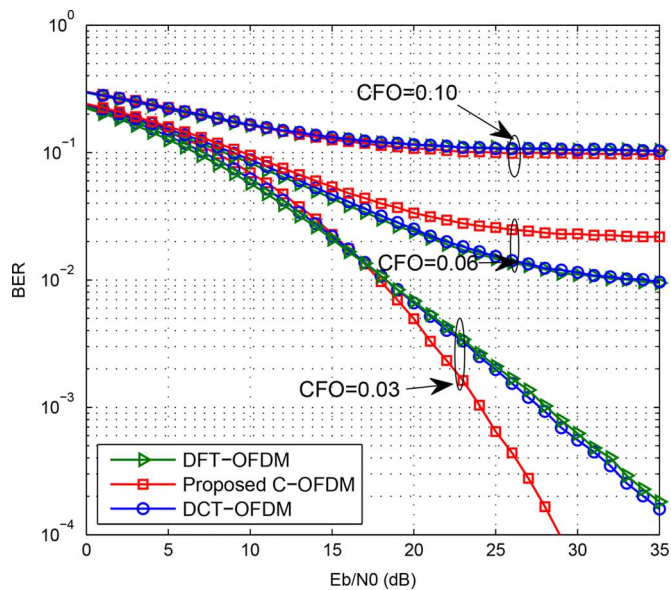


Fig. 9. BER performance of the proposed C-OFDM, DCT-OFDM and DFT-OFDM systems over ITU vehicular class A channel and CFO = 0.03, 0.06 and 0.1 and 16 QAM modulation format.

be extended beyond the wireless communications to include optical communication, the discrete multi-tone (DMT) and the PLC systems.

VII. CONCLUSION

In this paper, a new C-OFDM has been introduced using the IC/C transforms. The adoption of the C-transform in OFDM rather than the DCT or the DFT achieves better BER performance and PAPR reduction. It has been proved, mathematically and by simulation, that the C-OFDM can attain a valuable E_b/N_0 gain over the DCT-OFDM and DFT-OFDM systems when the ITU pedestrian and vehicular channel models are used. This is attributable to the use of the C-transform which has a block diagonal structure which results into better diversity and resilience against multipath channels.

Another advantage of the proposed C-OFDM system which has been explored in this paper is the PAPR reduction. Simulation results confirmed that the PAPR of the transmitted signal in the case of the C-OFDM system is lower than both the DCT-OFDM and DFT-OFDM. This is also due to the block-diagonal-structure of the C-transform, where the maximum signal superposition and the number of additions required for performing each C-OFDM sample is $\frac{N}{2}$ rather than N in the case of DCT-OFDM and DFT-OFDM. The range of applications of the proposed scheme can be extended beyond the wireless communications to include the discrete multi-tone (DMT) and the power line communication (PLC) system where signals are real not complex which is more suitable for C-OFDM.

REFERENCES

- [1] J. A. C. Bingham, "Multicarrier modulation for data transmission: An idea whose time has come," *IEEE Commun. Mag.*, vol. 28, pp. 5–14, 1990.
- [2] J. S. Chow, J. C. Tu, and J. M. Cioffi, "A discrete multitone transceiver system for HDSL applications," *IEEE J. Sel. Areas Commun.*, vol. 9, pp. 895–908, 1991.
- [3] H. Leftah and S. Boussakta, "Efficient modulation scheme for OFDM system with ZP and MMSE equalizer," in *Proc. IEEE Int. Conf. Commun. (ICC)*, Jun. 2013, pp. 4703–4707.
- [4] M. T. Hamood and S. Boussakta, "Fast Walsh-Hadamard-Fourier transform algorithm," *IEEE Trans. Signal Process.*, vol. 59, pp. 5627–5631, 2011.
- [5] M. Ahmed, S. Boussakta, B. Sharif, and C. Tsimenidis, "OFDM based on low complexity transform to increase multipath resilience and reduce PAPR," *IEEE Trans. Signal Process.*, vol. 59, no. 12, pp. 5994–6007, Dec. 2011.
- [6] W. Luqing and C. Tellambura, "Cross-entropy-based sign-selection algorithms for peak-to-average power ratio reduction of OFDM systems," *IEEE Trans. Signal Process.*, vol. 56, no. 10, pp. 4990–4994, 2008.
- [7] A. Al-Habashna, O. A. Dobre, R. Venkatesan, and D. C. Popescu, "Second-order cyclostationarity of mobile WiMAX and LTE OFDM signals and application to spectrum awareness in cognitive radio systems," *IEEE J. Sel. Topics Signal Process.*, vol. 6, no. 1, pp. 26–42, 2012.
- [8] S. Edinger, C. Bauer, and N. J. Fliege, "DMT transmission in the context of industrial telecontrol applications," *Adv. Radio Sci.*, vol. 4, pp. 155–160, Apr. 9, 2006.
- [9] O. Krajsa, P. Silhavy, and P. Sysel, "Filterbank modulation techniques and its utilization in ADSL systems," in *Proc. 34th Int. Conf. Telecommun. Signal Process.*, 2011.
- [10] Y. H. Ma, P. L. So, and E. Gunawan, "Performance analysis of OFDM systems for broadband power line communications under impulsive noise and multipath effects," *IEEE Trans. Power Del.*, vol. 20, no. 2, pp. 674–682, Apr. 2005.
- [11] K. Yong-Hwa and L. Jong-Ho, "Comparison of passband and baseband transmission schemes for power-line communication OFDM systems," *IEEE Trans. Power Del.*, vol. 26, no. 4, pp. 2466–2475, 2011.
- [12] S. Guruacharya, D. Niyato, D. I. Kim, and E. Hossain, "Hierarchical competition for downlink power allocation in OFDMA femtocell networks," *IEEE Trans. Wireless Commun.*, vol. 12, no. 4, pp. 1543–1553, Apr. 2013.
- [13] F. Cruz-Roldan, M. E. Dominguez-Jimenez, G. S. Vidal, P. Amo-Lopez, M. Blanco-Velasco, and A. Bravo-Santos, "On the use of discrete cosine transforms for multicarrier communications," *IEEE Trans. Signal Process.*, vol. 60, pp. 6085–6090, 2012.
- [14] B. Mathew, P. George, R. V. Nathan, S. Shukkor, and A. N. Lakshmi, "BER comparison of DCT and FFT based OFDM systems in AWGN and RAYLEIGH fading channels with different modulation schemes," in *Proc. Annu. Int. Conf. Emerg. Res. Areas/Int. Conf. Microelectron., Commun., Renewable Energy (AICERA/ICMiCR)*, 2013.
- [15] G. D. Mandyam, "On the discrete cosine transform and OFDM systems," in *Proc. IEEE Int. Conf. Acoust., Speech, Signal Process. (ICASSP)*, 2003.
- [16] T. Peng and N. C. Beaulieu, "Precise bit error probability analysis of DCT OFDM in the presence of carrier frequency offset on AWGN channels," in *Proc. IEEE Conf. Global Telecommun. (GLOBECOM)*, 2005.
- [17] C. Tao, G. Feifei, A. Nallanathan, and C. Tellambura, "ML CFO and PO estimation in DCT OFDM systems under non-circular transmissions," in *Proc. IEEE Int. Conf. Commun. (ICC)*, 2007.
- [18] G. D. Mandyam, "Sinusoidal transforms in OFDM systems," *IEEE Trans. Broadcast.*, vol. 50, no. 2, pp. 172–184, 2004.
- [19] N. C. Beaulieu and P. Tan, "Systems and methods for OFDM transmission and reception," U.S. Patent 0095267 A1, 2008.
- [20] T. Peng and N. C. Beaulieu, "A comparison of DCT-based OFDM and DFT-based OFDM in frequency offset and fading channels," *IEEE Trans. Commun.*, vol. 54, no. 11, pp. 2113–2125, 2006.
- [21] G. Feifei, C. Tao, A. Nallanathan, and C. Tellambura, "Maximum likelihood based estimation of frequency and phase offset in DCT OFDM systems under non-circular transmissions: Algorithms, analysis and comparisons," *IEEE Trans. Commun.*, vol. 56, no. 9, pp. 1425–1429, 2008.
- [22] P. Tan and N. C. Beaulieu, "An improved DCT-based OFDM data transmission scheme," in *Proc. IEEE 16th Int. Symp. Personal, Indoor, Mobile Radio Commun. (PIMRC)*, 2005.
- [23] A. Ruzhdi and J. Tuqan, "PAPR reduction in trigonometric-based OFDM systems," in *Proc. 41st Asilomar Conf. Signals, Syst., Comput. (ACSSC)*, 2007.

- [24] N. Al-Dhahir, M. Hlaing, and S. Satish, "Optimum DCT-based multicarrier transceivers for frequency-selective channels," *IEEE Trans. Commun.*, vol. 54, no. 5, pp. 911–921, 2006.
- [25] D. Hein and N. Ahmed, "On a real-time WalshHadamard/cosine transform image processor," *IEEE Trans. Electromagn. Compat.*, EMC-20, no. 3, pp. 453–457, 1978, vol., pp..
- [26] Y. Tanabe, Y. Egashira, and K. Sato, "A novel IQ imbalance estimation scheme using transient local frequency for OFDM systems," in *Proc. IEEE Int. Symp. Personal, Indoor, Mobile Radio Commun. (PIMRC)*, 2007.
- [27] B. Muquet, W. Zhengdao, G. B. Giannakis, M. de Courville, and P. Duhamel, "Cyclic prefixing or zero padding for wireless multicarrier transmissions," *IEEE Trans. Commun.*, vol. 50, no. 12, pp. 2136–2148, 2002.
- [28] W. Zhendao and G. B. Giannakis, "Wireless multicarrier communications," *IEEE Signal Process. Mag.*, vol. 17, no. 3, pp. 29–48, 2000.
- [29] J. G. Proakis and M. Salehi, *Digital Communications*. New York, NY, USA: McGraw-Hill, 2008.
- [30] C. Tellambura, "Use of m-sequences for OFDM peak-to-average power ratio reduction," *Electron. Lett.*, vol. 33, pp. 1300–1301, 1997.
- [31] E. Costa and S. Pupolin, "M-QAM-OFDM system performance in the presence of a nonlinear amplifier and phase noise," *IEEE Trans. Commun.*, vol. 50, no. 3, pp. 462–472, 2002.
- [32] V. Britanak, P. Yip, and K. R. Rao, *Discrete Cosine and Sine Transforms: General Properties, Fast Algorithms and Integer Approximations*. Amsterdam, The Netherlands: Academic, 2007.
- [33] G. H. Golub and C. F. V. Loan, *Matrix Computation*, 3rd ed. Baltimore, MD, USA: The Johns Hopkins Univ. Press, 1996.



Hussein A. Leftah received the B.Sc. (with the first rank of 85) and M.Sc. degrees in electrical engineering from Basrah University, Iraq, in 2002 and 2004, respectively. He received his Ph.D. degree in electrical and electronic engineering from Newcastle University, Newcastle Upon Tyne, England, in 2013.

Mr. Leftah is currently a Lecturer at Electrical department, Southern Technical University, Basrah, Iraq. His current research interests include Digital signal processing for communication, OFDM systems, power line communication and optical communication.



Said Boussakta (SM'04) received the "Ingenieur d'Etat" degree in electronic engineering from the National Polytechnic Institute of Algiers, Algeria in 1985 and the Ph.D. degree in electrical engineering from Newcastle University, U.K., in 1990.

From 1990–1996, he was with Newcastle University as a Senior Research Associate in Digital Signal Processing. From 1996–2000, he was with the University of Teesside, U.K., as a Senior Lecturer in Communication Engineering. From 2000–2006, he was at the University of Leeds as a Reader in Digital Communications and Signal Processing. He is currently a Professor of Communications and Signal Processing and Head of the Communications, Sensors and Signal Processing (CSSP) Group at the School of Electrical and Electronic Engineering, Newcastle University, where he is lecturing in Communication Networks and Signal Processing subjects. His research interests are in the areas of fast DSP algorithms, Digital Communications, Communication Network Systems, Cryptography, and Digital Signal/Image Processing. He has authored and co-authored more than 200 publications and served as Chair for Signal Processing for Communications Symposium in ICC'06, ICC'07, ICC'08, ICC'10 and ICC'13.

Prof. Boussakta is a Fellow of the IET, and a Senior Member of the Communications and Signal Processing Societies.